The Meteoritical Society

Meteoritics & Planetary Science 52, Nr 7, 1330–1350 (2017)
doi: 10.1111/maps.12825

Complex crater formation: Insights from combining observations of shock pressure distribution with numerical models at the West Clearwater Lake impact structure

A. S. P. RAE[1,*], G. S. COLLINS[1], R. A. F. GRIEVE[2], G. R. OSINSKI[2,3], and J. V. MORGAN[1]

[1]Department of Earth Science and Engineering, Imperial College London, London SW7 2BP, UK
[2]Department of Earth Sciences/Centre for Planetary Science and Exploration, University of Western Ontario, London, Ontario N6A 5B7, Canada
[3]Department of Physics and Astronomy, University of Western Ontario, London, Ontario N6A 5B7, Canada
[*]Corresponding author. E-mail: a.rae14@imperial.ac.uk

(Received 15 March 2016; revision accepted 11 December 2016)

Abstract–Large impact structures have complex morphologies, with zones of structural uplift that can be expressed topographically as central peaks and/or peak rings internal to the crater rim. The formation of these structures requires transient strength reduction in the target material and one of the proposed mechanisms to explain this behavior is acoustic fluidization. Here, samples of shock-metamorphosed quartz-bearing lithologies at the West Clearwater Lake impact structure, Canada, are used to estimate the maximum recorded shock pressures in three dimensions across the crater. These measurements demonstrate that the currently observed distribution of shock metamorphism is strongly controlled by the formation of the structural uplift. The distribution of peak shock pressures, together with apparent crater morphology and geological observations, is compared with numerical impact simulations to constrain parameters used in the block-model implementation of acoustic fluidization. The numerical simulations produce craters that are consistent with morphological and geological observations. The results show that the regeneration of acoustic energy must be an important feature of acoustic fluidization in crater collapse, and should be included in future implementations. Based on the comparison between observational data and impact simulations, we conclude that the West Clearwater Lake structure had an original rim (final crater) diameter of 35–40 km and has since experienced up to ~2 km of differential erosion.

INTRODUCTION

Complex crater formation requires a significant and transient reduction in the strength of target rocks compared to their quasistatic strengths (Melosh 1989). The mechanism of this weakening remains unresolved despite over 40 years of research; as such, understanding the dynamics of complex crater collapse is one of the primary aims of impact cratering research (Kenkmann et al. 2012). For large terrestrial craters, the effective strength required for the formation of central uplifts and crater collapse must be less than ~3 MPa and there must be little or no internal friction (Melosh 1977; McKinnon 1978; O'Keefe and Ahrens 1999; Wünnemann and Ivanov 2003). These properties are inconsistent with laboratory measurements of the properties of rocks and even those of damaged rocks. Therefore, there must be an additional mechanism or mechanisms that facilitate complex crater collapse.

One of the proposed mechanisms to explain transient weakening during impact crater collapses is acoustic fluidization (Melosh 1979). In this model, short-wavelength elastic waves, produced by either the passage of the shock wave or subsequent deformation, cause a release of overburden pressure in the deforming material. Rocks, and other brittle materials, behave as a Coulomb material; that is, the yield strength of the material is directly proportional to the overburden pressure. The constant of proportionality between these two properties is the coefficient of internal friction, μ. Consequently, a release of overburden pressure due to vibrations in the material would be expected to cause

reduction in the yield strength of the material (Melosh and Ivanov 1999).

The acoustic fluidization model is commonly used in numerical simulations of complex crater collapse and has had considerable success in replicating the size-morphology progression of terrestrial and lunar craters (Collins 2014; Baker et al. 2016), as well as modeling the specific features of individual craters (e.g., Collins et al. 2002, 2008a; Wünnemann et al. 2005; Goldin et al. 2006; Vasconcelos et al. 2012). Despite these successes, a considerable limitation of impact simulations that employ acoustic fluidization is non-uniqueness. In producing final crater sizes and morphologies, there are trade-offs between impactor size and acoustic fluidization parameters and, more importantly, there are trade-offs between the acoustic fluidization parameters themselves (Wünnemann and Ivanov 2003). For example, Wünnemann and Ivanov (2003) showed that the same crater size-morphology progression can be produced with short-lived, low-viscosity fluidization or long-lived, high-viscosity fluidization. Reducing the non-uniqueness of numerical impact simulations requires multiple quantitative observational data sets. A further challenge of the acoustic fluidization model is the relationship between observable target properties, such as the size of discrete rock blocks, with the parameters of the model (e.g., Ivanov and Artemieva 2002).

Here, predictions obtained from numerical models of the formation of the West Clearwater Lake impact structure, Canada, are compared with geological observations; in particular, core logging, field observations, and shock barometry, with the aim of constraining the model parameters describing acoustic fluidization and, hence, the kinematics and dynamics of complex crater formation.

Shock Barometry

One of the primary challenges in assessing the validity of acoustic fluidization is in the uncertainties regarding the kinematics of complex crater collapse. This is particularly challenging in crystalline target rocks, where there are no stratigraphic markers to identify the original position of material. However, the final distribution of shock metamorphism in complex craters provides a possible constraint on the kinematics of crater modification (Dence 2004). At the point in time when the transient cavity is fully formed, shock isobars are arranged approximately concentrically around the transient cavity; from this point, the transient cavity undergoes modification to form the final crater. By analyzing the distribution of shock metamorphism in three dimensions, constraints can be placed upon the kinematics of crater modification (e.g., Ivanov 1994).

Previous studies have shown that quartz is a particularly useful mineral for shock barometry. It is both very stable and abundant in terrestrial rocks, and it also displays a variety of shock metamorphic effects dependent upon the magnitude of the peak pressure (Grieve et al. 1996). Notably, quartz displays the development of planar deformation features (PDFs) oriented along different crystallographic planes dependent upon the peak shock pressure (Carter 1965; Hörz 1968; Müller and Défourneaux 1968; Huffman and Reimold 1996). By characterizing the orientations of PDFs, the degree and extent of shock metamorphism can be determined at impact structures, for example, Charlevoix, Manicouagan, Slate Islands, and Siljan (Robertson 1975; Grieve and Robertson 1976; Robertson and Grieve 1977; Dressler et al. 1998; Holm et al. 2011). Furthermore, the observation of other shock related features: shatter cones, planar fractures (PFs) in quartz, diaplectic quartz and feldspar glasses, and feather features (FFs) in quartz can indicate shock pressure magnitudes (see French and Koeberl 2010).

West Clearwater Lake Impact Structure

Located in northern Quebec, Canada (Fig. 1), Clearwater Lake is composed of two broadly circular lobes; each lobe is a distinct impact structure. The smaller structure, East Clearwater Lake, is generally described as a 24 km diameter central-peak crater. The larger structure, West Clearwater Lake, is generally described as a 32 km diameter peak-ring crater; however, there has been some discussion that this diameter represents only a minimum value (see Grieve 2006). The structures were first suggested as a pair of impact craters by Beals et al. (1956). Subsequent work through the 1960s debated an impact or volcanic origin for the structures (Kranck and Sinclair 1963; Dence 1964; Dence et al. 1965; Bostock 1969), and during this time five drill cores from West Clearwater Lake were recovered by the Dominion Observatory. Concurrently, PDFs were beginning to be recognized as unique shock-metamorphism indicators and were observed in breccias at West Clearwater Lake (Engelhardt et al. 1968), proving an impact origin of the structures. Further field work and petrologic studies (Phinney et al. 1978; Simonds et al. 1978; Hische 1994) have confirmed an impact origin. The geology and history of study of the Clearwater Lake impact structures are comprehensively reviewed in Grieve (2006). Recent (U-Th)/He and $^{40}Ar/^{39}Ar$ dating (Schmieder et al. 2015; Biren et al. 2016) indicates that the impact events at Clearwater are noncoeval. East Clearwater Lake is 460–470 Ma old

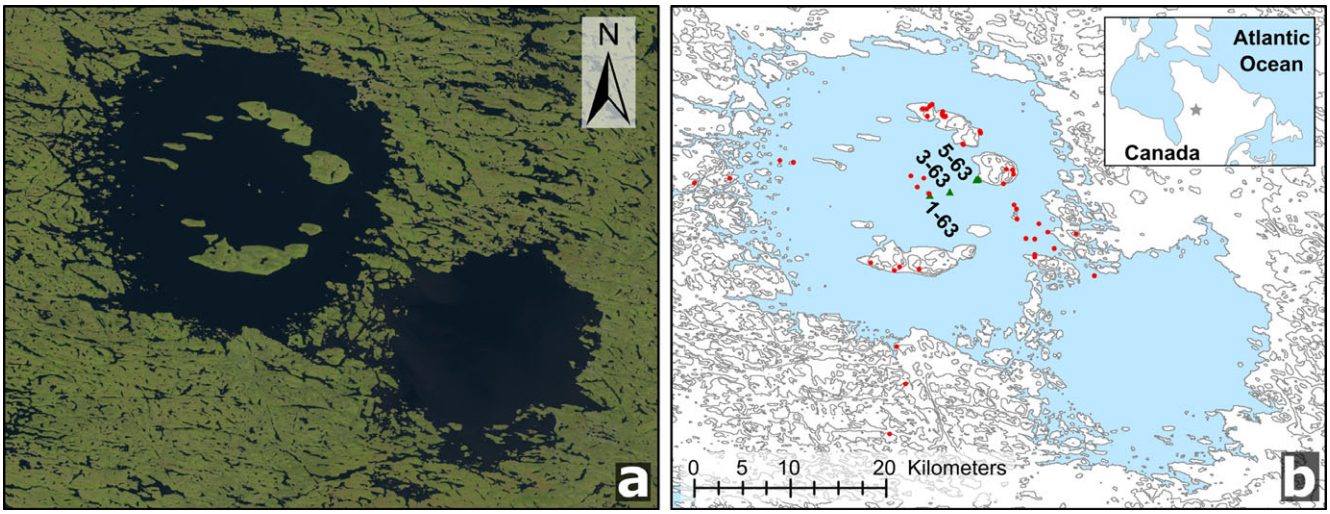

Fig. 1. The Clearwater Lake impact structures. a) Satellite image of Clearwater Lake taken by Landsat (Image Source: Landsat Operational Land Imager/USGS). b) Outline map of Clearwater Lake, contours are in intervals of 50 m above lake level. Red dots indicate the location of samples used in this study, green triangles indicate the location of recovered drill cores. Core 4-63 is located close to core 5-63 (Data source: CDED, GeoBase Canada). (Color figure can be viewed at wileyonlinelibrary.com.)

(Ordovician), whereas West Clearwater Lake is 286 ± 2.2 Ma old (Permian). Previous dating of the structures had suggested that both impact events occurred at 285–300 Ma ago (Reimold et al. 1981) as a consequence of the impact of a binary asteroid (Dence et al. 1965).

West Clearwater Lake has a well-exposed island ring between 6–11 km from the center of the structure, preserving impact-melt rocks, impact breccias, and some intact para-autochthonous basement rocks. The target rocks were amphibolite- to granulite-facies metamorphosed granites, granodiorites, tonalites, and felsic gneisses, with local mafic amphibolites belonging to the 2.6–2.8 Ga Archean Bienville Sub-province of the Superior Province of the Canadian Shield. A thin, possibly non-uniqueness, veneer of Ordovician limestone, subsequently eroded away from the local area, overlay the basement rocks at the time of impact. There are no specific estimates of the amount of erosion that Clearwater Lake has experienced since the time of impact. Impactites include shocked crystalline basement and breccias containing shocked quartz (Engelhardt et al. 1968) and shatter cones (Dence 1964), impact-melt-bearing breccias, and the lower part of a coherent impact-melt sheet (Phinney et al. 1978; Simonds et al. 1978; Hische 1994; Rosa 2004, 2011). Estimates of the original melt volume at West Clearwater Lake range from 68 km^3 to 100 km^3 (Grieve et al. 1976; Phinney and Simonds 1977). There is no indication of the admixture of identifiable meteoritic material within the impact-melt rock at West Clearwater Lake (Grieve 1978; Palme et al. 1978).

METHODS

Samples

Sixty samples of exposed bedrock were recovered from the West Clearwater Lake structure during a field campaign in the summer of 2014. For this study, only basement rocks were sampled. The sampled lithologies represent granites, granodiorites and tonalites, and occasional mafic amphibolites. In hand-specimen, the felsic samples are medium to very coarse-grained, are gray to reddish-gray in color, and can be quite friable. Samples were recovered from localities interpreted to be para-autochthonous spread across the structure, although in some areas determining whether the outcropping basement material was part of an allochthonous megablock within the impact-melt sheet or part of the para-autochthon was challenging. The occurrence of shatter cones was noted around the structure.

In addition, five recovered drill cores from West Clearwater Lake were logged. These drill cores were recovered in the winter of 1963 by the Dominion Observatory and are now housed at the Natural Resources Canada core facility in Ottawa. The locations of the cores are indicated on Fig. 1. Core 1-63, in the center of the structure, reached 397.3 m (1307 ft) depth; core 3-63, reached 394.3 m (1297 ft) depth; core 5-63 reached a depth of 219.5 m (722 ft); and cores 4-63 and 4a-63 reached depths of 119.2 m (392 ft) and 64.4 m (212 ft), respectively. Samples were used from cores 1-63, 3-63, and 5-63 for shock analysis; cores 4-63 and

4a-63 did not drill deep enough to sample a significant amount of para-autochthonous lithologies.

Shock Barometry

In total, 149 thin sections of para-autochthonous lithologies were petrographically analyzed. Of these, 60 thin sections derived from the field samples and 89 thin sections derived from the drill cores. Forty-seven field thin sections and 70 drill core thin sections contained quartz and were studied with respect to characterizing PDFs in quartz. The thin sections were first characterized based on mineral assemblage and searched for shock metamorphic features with an optical microscope. A more detailed study of these thin sections to characterize PDF orientations was achieved using a Zeiss 4-axis Universal stage following the techniques described in Engelhardt and Bertsch (1969), Stöffler and Langenhorst (1994), and Ferrière et al. (2009). Analysis of PDF orientations requires the measurement of the orientation of the optic axis and the poles to all PDF planes in an individual quartz grain by the use of a universal stage. These measurements were used to index the PDFs to specific crystallographic planes with the use of a stereographic projection template. Here, the program ANIE v1.1 (Huber et al. 2011) was used to index PDFs after cross-checking against plotting the PDFs manually using the new stereographic projection template (NSPT) of Ferrière et al. (2009).

During indexing, a 5° envelope is allowed to account for errors in measurement and for the slight variation of crystallographic orientation between domains of the crystal. There is an overlap between the 5° error envelopes of the $\{10\bar{1}3\}$ and $\{10\bar{1}4\}$ PDF orientations. Here, if the pole to a PDF plane plotted within this region, it was considered to be in the $\{10\bar{1}3\}$ orientation.

In order to ensure reliable pressure estimates based on the PDF data, a sufficient number of quartz grains need to be measured (Ferrière et al. 2009). Here, 30 quartz grains were measured per sample, where possible. In samples with less than 30 quartz grains, all quartz grains were analyzed, with a minimum number being 17 grains. Quartz grains were included in the pressure estimates regardless of whether or not they contained PDFs.

Shock pressure estimates were made based on the indexed PDF orientations. Here, the method of Robertson and Grieve (1977) was used. Each quartz grain was assigned a shock pressure based on which PDF sets it contained, the shock calibration scheme used here is based on the scheme suggested by Stöffler and Langenhorst (1994) and Grieve et al. (1996) and presented in Table 1. The shock pressure of the sample was then calculated by taking the arithmetic mean of the individually assigned shock pressures within the sample.

Table 1. Shock classification scheme, based on Stöffler and Langenhorst (1994) and Grieve et al. (1996).

Observation	Shock pressure range (GPa)	Median shock pressure (GPa)
No. of observed PDFs, within shatter cone radius	2–5	3.5
(0001)	5–10	7.5
$\{10\bar{1}3\}$	10–20	15
$\{10\bar{1}2\}$	20–35	27.5
Diaplectic quartz glass	>35	—

Numerical Modeling

Simulations of the formation of the West Clearwater impact structure were achieved using the iSALE shock physics code. iSALE is a multirheology, multimaterial code based on the SALE hydrocode (Amsden et al. 1980). Modifications to the original code have included an elastoplastic constitutive model, fragmentation models (Melosh et al. 1992), various equations of state (Ivanov et al. 1997), a porous compaction model (Wünnemann et al. 2006), and a dilatancy model (Collins 2014). The iSALE (and the closely related SALE-B) code has been used to model several terrestrial impact structures: Chesapeake Bay (Collins and Wünnemann 2005; Kenkmann et al. 2009), Ries (Wünnemann et al. 2005; Collins et al. 2008a), Sierra Madera (Goldin et al. 2006), Chicxulub (Ivanov 2005; Collins et al. 2008b), and Haughton and El'gygytgyn (Collins et al. 2008a).

Here, models of the West Clearwater Lake impact event were carried out with the aim of investigating the effect of acoustic fluidization parameters on shock pressure distribution. Consequently, all impact model parameters, other than acoustic fluidization parameters, were kept constant between different simulations. The target consists of crystalline granitic basement; we assume that the sedimentary cover at the time of impact was negligible. As there is no indication of the impactor composition at West Clearwater Lake, a granitic impactor was used for computational efficiency and because the density of granite is representative of stony meteorites. Due to the axisymmetric nature of the model, the angle of impact in all simulations was perpendicular to the target surface, significantly steeper than the most likely angle of 45°. To crudely account for this discrepancy in probable impact angle, we used

an impactor velocity of 15 km s^{-1}, which is approximately equal to the vertical velocity component of an impactor striking at 45° to the surface with a speed of 20.5 km s^{-1} (Le Feuvre and Wieczorek 2011), the average asteroid collision speed on Earth. Final crater size has been shown to scale with the vertical component of impact velocity, rather than the direct velocity (Chapman and McKinnon 1986; Elbeshausen et al. 2009). Adopting a slightly lower impact velocity also increases computational efficiency in that it reduces the volume of vaporized rock. A nominal impactor diameter of 3 km was chosen, such that a structure of approximately the correct proportions was formed, and that models with different acoustic fluidization parameters were directly comparable. We note that the impactor parameters and acoustic fluidization parameters trade-off against each other to produce a crater of a specific size, creating uncertainty in the final acoustic fluidization parameters. Furthermore, the symmetry of the shock pressure distribution would be affected by a nonvertical impact. Nonetheless, for a reasonable range of impactor parameters, at fixed acoustic fluidization parameters, the process of crater collapse is qualitatively identical, although the final crater size varies (see Video S1 in supporting information). The atmosphere was not included in our models. The important parameters for the models are included in Table 2. To track the peak shock pressure of material in the model, Lagrangian tracer particles were used. These are marker particles, inserted into the computational grid at the start of the simulation which, as the simulation progresses, move with the material flow without interacting with it and recording the position and thermodynamic history of the material package (e.g., Pierazzo et al. 1997; Collins et al. 2008a).

Table 2. iSALE parameters.

Symbol	Definition	Value
L	Impactor diameter (km)	3.0
v_i	Impact velocity (km s^{-1})	15.0
ρ_i	Impactor density (kg m^{-3})	2630
ρ_t	Target density (kg m^{-3})	2630
ν	Poisson's ratio	0.3
Y_0	Cohesion (MPa)	10
Y_M	Von Mises plastic limit (MPa)	2500
μ_i	Coefficient of internal friction	2
Y_{d0}	Cohesion of damaged material (MPa)	0.01
μ_{di}	Coefficient of internal friction of damaged material	0.6
Tm	Melting temperature (K)	1673
ξ	Thermal softening parameter	1.2
ε_{fb}	Minimum failure strain for low pressure states	1×10^{-4}
B	Constant of proportionality between failure strain and pressure	1×10^{11}
P_c	Pressure above which failure is compressional (Pa)	3×10^{8}
C_{vib}	Vibrational particle velocity as a fraction of particle velocity	0.1
Vib_{max}	Maximum vibrational particle velocity (m s^{-1})	200
t_{off}	Time after which no new acoustic vibrations are generated (s)	16

The thermodynamic behavior of the materials in the model is described by an equation of state (EoS). We used tables generated using the Analytic EoS program (ANEOS, Thompson and Lauson 1974) for granite using input parameters described in Pierazzo et al. (1997).

The constitutive model used accounts for changes in material shear strength that result from changes in pressure, temperature, and damage (Ivanov et al. 1997). The strength parameters used for the granitic crystalline basement in our simulations were based on those used in previous models (e.g., Wünnemann et al. 2005). The constitutive model is supplemented by the block model of acoustic fluidization, a transient weakening model, such that gravitational collapse of the transient cavity is facilitated (Melosh 1989; Melosh and Ivanov 1999). The parameters of the constitutive model between all simulations were fixed, varying these parameters would change the distribution and magnitude of damage. As acoustic fluidization only occurs where material is damaged, this would affect where acoustic fluidization is able to reduce strength. As such, there is a small trade-off between these parameters and the acoustic fluidization parameters.

The block model of acoustic fluidization (Ivanov and Kostuchenko 1997) is a simplification of the full model of acoustic fluidization. The block model is motivated by observations of the Putchez-Katunki deep drill core (Ivanov et al. 1996), where discrete rock blocks were observed to be separated by interblock breccias. The block model is an attempt to reconcile direct, and measurable, geological observations of the central uplifts of complex craters to the parameters of numerical models. The block-oscillation model produces a rheology with a time-dependent yield strength and a constant effective viscosity, η; that is, a time-varying Bingham fluid rheology. As time evolves, the strength of the fluidized material increases as vibrational energy decays exponentially, with decay time constant T_{dec}. The two important block model parameters, η and T_{dec}, must scale in some way with a physically observable parameter, such as the characteristic block size. Several impact modeling studies (Wünnemann and Ivanov 2003; Collins 2014; Baker et al. 2016) have shown that the

size-morphology progression of craters on Earth and the Moon is well produced by assuming a linear proportionality between impactor size and both η and T_{dec}. Following the definitions of Wünnemann and Ivanov (2003), we adopt:

$$\eta = \gamma_\eta c_s r \rho \quad \text{and} \quad T_{dec} = \gamma_T \frac{r}{c_s} \tag{1}$$

where c_s is the bulk sound speed, r is the impactor radius, and ρ is the material density. γ_η and γ_T are dimensionless scaling constants.

Effective viscosity and decay time can be converted to block size, h, and quality factor for acoustic attenuation, Q, under several assumptions. In one approximation, harmonic motion of blocks is assumed, where the oscillation period is controlled by the compressibility and thickness of the interblock matrix relative to the blocks and is proportional to block size (Ivanov and Artemieva 2002). In this case, both effective viscosity and decay time are proportional to block size h and the quality factor Q is proportional to the ratio η/T_{dec}. The validity of this scaling requires the time taken for sound to cross a block to be shorter than the period of the block oscillation; that is, compared to the blocks, the breccia must be significantly thick (~10% of the block size) and compressible (~2 × that of the block).

RESULTS

Observations

Macroscopic

Fieldwork in summer 2014 demonstrated that the stratigraphy preserved at West Clearwater Lake consists of (a) fractured basement, (b) monomict lithic breccia, (c) impact-melt-bearing lithic breccia, (d) clast-rich fine-grained impact-melt rock, (e) clast-poor fine-grained impact-melt rock, and (f) clast-poor medium-grained impact-melt rock (Osinski et al. 2015), similar to the identified stratigraphies of Bostock (1969) and Simonds et al. (1978). Structural mapping of these lithologies indicates that the para-autochthonous-allochthonous contact, between the fractured basement and overlying units, is located at, or near, lake level around the ring structure. Most of the verifiably para-autochthonous basement material is located on shoreline exposures, while occasional outcrops inland either reflect a rugged basement topography or are actually allochthonous mega-blocks. The island ring has ~100 m of topography (relative to lake level) and, at the present level of exposure, is composed largely of impact-melt rocks and some impact breccias.

The small islands located in the center of the structure (Fig. 1b) are composed of para-autochthonous, fractured basement. The fractured basement commonly has poorly developed shatter cones (Fig. 2), from the center of the structure and beyond the extent of the island ring to ~11 km radial distance. On the central islands, the contact with allochthonous lithologies is located somewhere above the present day exposure, that is, all allochthonous lithologies were eroded from the center of the structure. Furthermore, no impact ejecta was found toward the rim of the structure.

The drill cores confirm that, at the island ring, the para-autochthonous contact is located near to lake level (39.7 m below lake level in core 5-63 and 64.1 m below lake level in core 4-63), while cores 1-63 and 3-63 show only para-autochthonous rocks. The basement rocks show clear evidence of deformation; in the form of breccias, melt veins, and cataclasites (Figs. 2 and 3). Deformation is, in general, most pervasive in the central drill cores and toward the top of the cores. Individual deformation bands are narrow; melt veins are particularly common, <1 cm wide and, in most cases, have no discernable displacement. Cataclasites are <10 cm wide and vary significantly in maturity, from protocataclasites to ultracataclasites that occasionally contain within them pseudotachylites. Breccias are rare in the drill core, are <50 cm wide, and commonly have melt matrixes. Breccias and melt veins were observed in the field (Wilks and Osinski 2015) (Fig. 2); however, exposure of the fractured basement was too limited to map individual blocks. Nonetheless, estimates of block size and matrix thickness can be made based on the drill core logs (Fig. 3).

Block sizes in the drill cores were estimated by measuring the distance between each separate discontinuity, with the discontinuity being either a cataclasite, melt vein, or breccia. A significant number of discontinuities, particularly the melt veins, have likely seen no displacement indicating that block sizes would be underestimated. Conversely, deformation zones are undersampled; there are significant sections of core that have poor or no core recovery, it is likely that the cause of these missing sections of rock is that they contain a greater concentration of deformation zones, which would lead to block size overestimation. Thus, only crude estimates of the block size were possible. Across all the cores, the average block size is 12 m with the largest block ~43 m and the smallest block <1 m. The average block size in core 1-63 is ~10 m compared to ~14 m in cores 3-63 and 5-63.

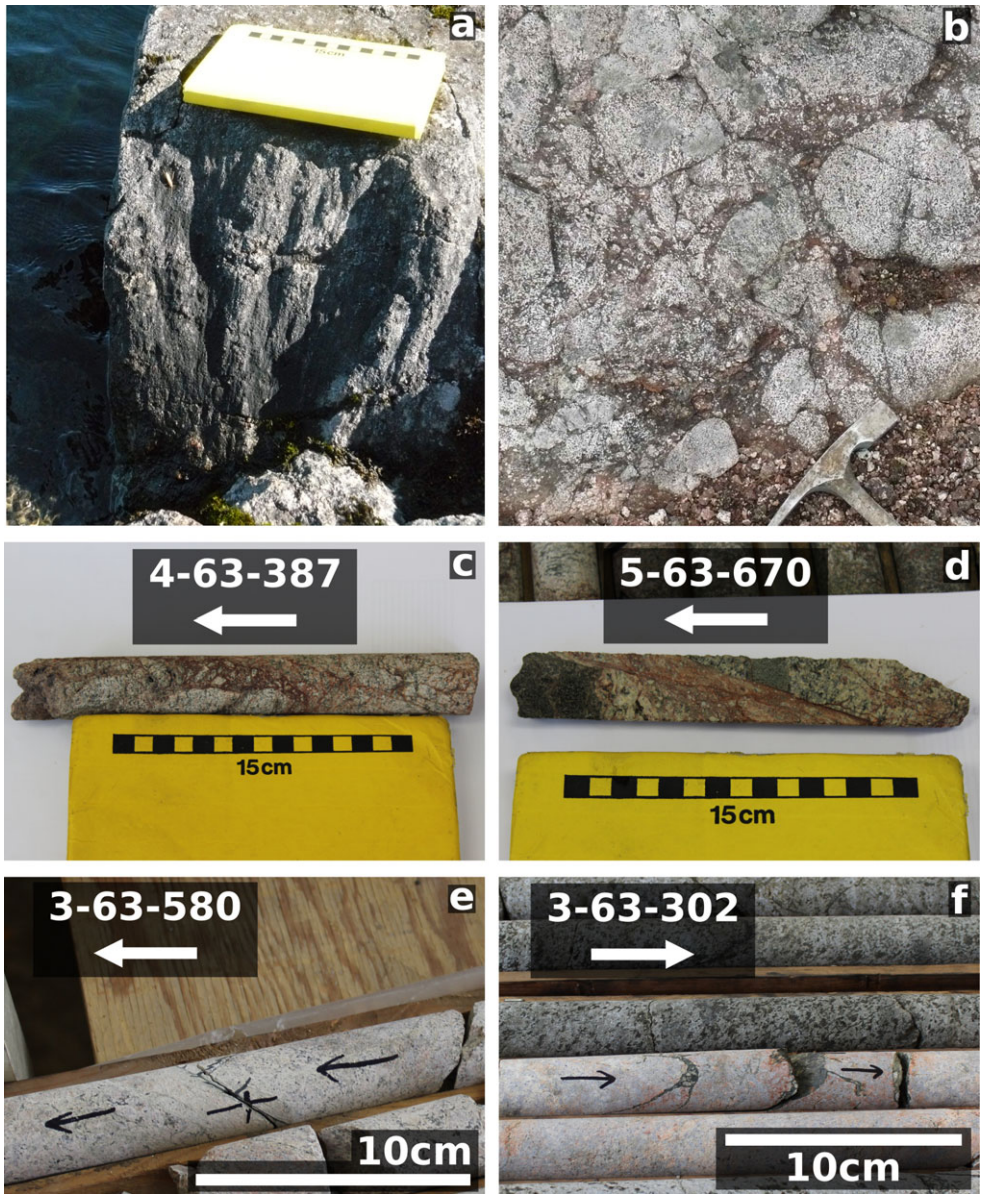

Fig. 2. Macroscopic products of impact deformation. a) Shatter cone. b) Breccia dike with melt matrix emplaced into intact crystalline basement. c) Pseudotachylitic impact breccia. d) Cataclastic displacement zone. e) Cataclasite and associated pseudotachylite. f) Solidified impact-melt veins. Arrow indicates the up direction of the drill core, sample names indicate the core followed by the depth in feet from the lake surface for example, 4-63-387 is from core 4-63 at a depth of 387 feet. (Color figure can be viewed at wileyonlinelibrary.com.)

Petrographic Description

The felsic basement rocks contained abundant shock metamorphic features in quartz, particularly PDFs, alongside planar fractures (PFs), and feather features (FFs). Furthermore, kink banding in biotite and occasional PDFs in plagioclase feldspars were observed (Fig. 4). A complete table of PDF statistics can be found in Data S1 in supporting information, and summarized in Table 3. Between 0 and 5 PDF sets were observed per quartz grain with the average number of PDFs per grain in a sample ranging from 0 to 2.17 (Table 3). The PDF sets are generally decorated although some samples show undecorated PDFs. As samples become less shocked, PDFs are less well developed; in particular, poorly shocked samples rarely have PDFs across the entire width of the grain.

In overall abundance, (0001) orientations account for 36.5% of the total measured planes, $\{10\bar{1}4\}$ account for 11.5%, $\{10\bar{1}3\}$ account for 27.1%, $\{10\bar{1}2\}$ account for 4.6%, and the remaining orientations

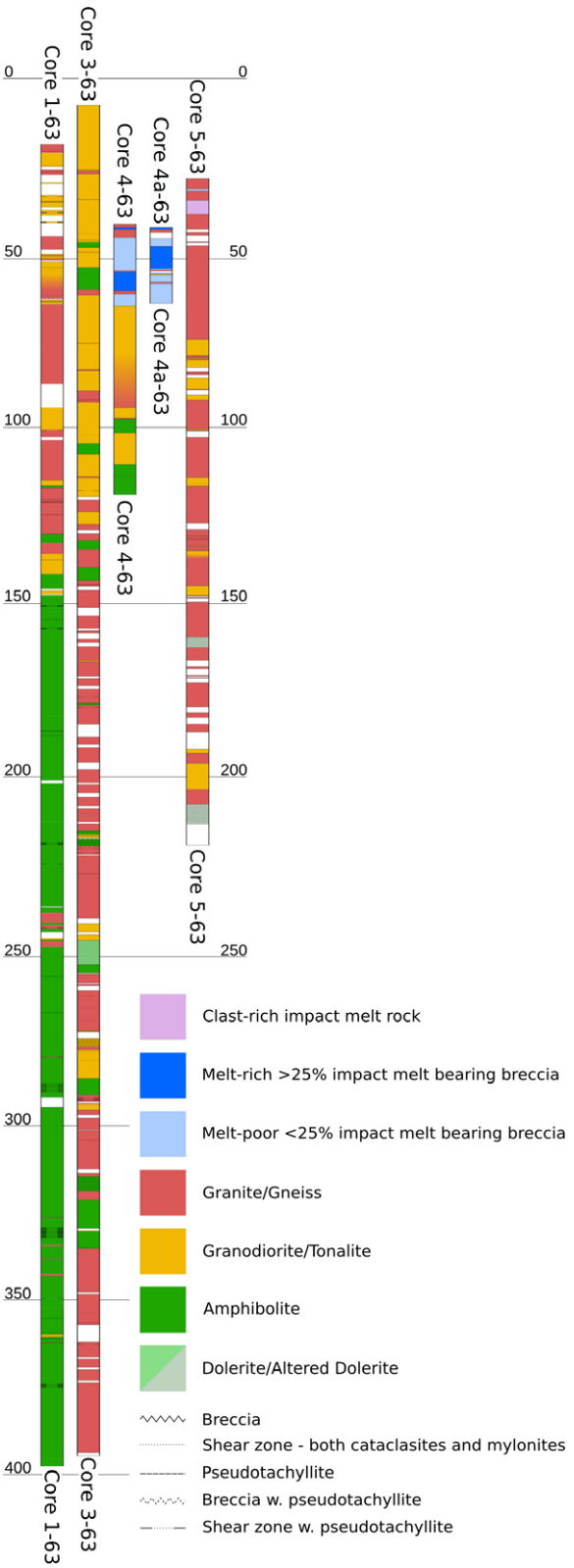

Fig. 3. Drill core logs of all the cores from West Clearwater Lake, describing both lithological and structural features. Depth is indicated in meters below lake level. (Color figure can be viewed at wileyonlinelibrary.com.)

account for the remaining 9.0% (Table 3). Approximately 11% of measured planes could not be indexed. This either reflects human error in the original measurements or that there are possible PDF planes not included in the New Stereographic Projection Template (NSPT) (Ferrière et al. 2009).

PFs in quartz occur infrequently as open, and widely (0.1 mm–1 mm) spaced fractures. These PFs were generally, but not exclusively, observed parallel to the (0001) plane. Feather feature lamellae were occasionally observed against planar fractures.

Other impact-related features observed in the samples include melt veins and cataclasites. In many cases, except for ultracataclasites, shocked quartz grains can be identified within the cataclastic zone. Here, PDFs were measured and oriented, although care was taken to avoid remeasuring a PDF orientation in a grain fragment that had already been measured in a different fragment. Shocked quartz was not observed in the melt veins.

Most of the mafic lithologies analyzed showed no definitive shock metamorphic effects. Only one section, from the center of structure, contained a partially diaplectic plagioclase feldspar glass (Fig. 4).

Shock Barometry

Pressure estimates based on the measured PDF data are shown in Figs. 5 and 6. In general, shock decreases as a function of distance from the center. Among the surface samples, shock pressures are relatively constant (~17.5 GPa) across the center of the structure until ~8 km radial distance, where the number of PDFs drops almost immediately to zero; no PDFs were observed in any samples beyond ~8.5 km radial distance. Field observations suggest that the radial extent of shatter cones is 11 km.

These results are consistent with shock pressures estimated from the drill cores. Where, at the top of each drill core, shock pressure estimates based on the shock metamorphism of quartz are ~17.5 GPa. In all drill cores, there is a general trend toward shock pressures decreasing with depth. This is most apparent in core 5-63, located at the greatest radial distance, where no PDFs are observed toward the bottom of the core at >150 m depth. Shock pressure attenuates at the lowest rate in the most central core, 1-63, while shock attenuates at an intermediate rate in core 3-63. The mean standard deviation for all of the pressure estimates is 4.0 GPa (see Data S1).

There is a good correlation between shock pressure and the average number of PDFs per grain (Fig. 7), confirming that the number of PDFs per grain could be used as a proxy for peak shock pressure (Ferrière et al. 2008).

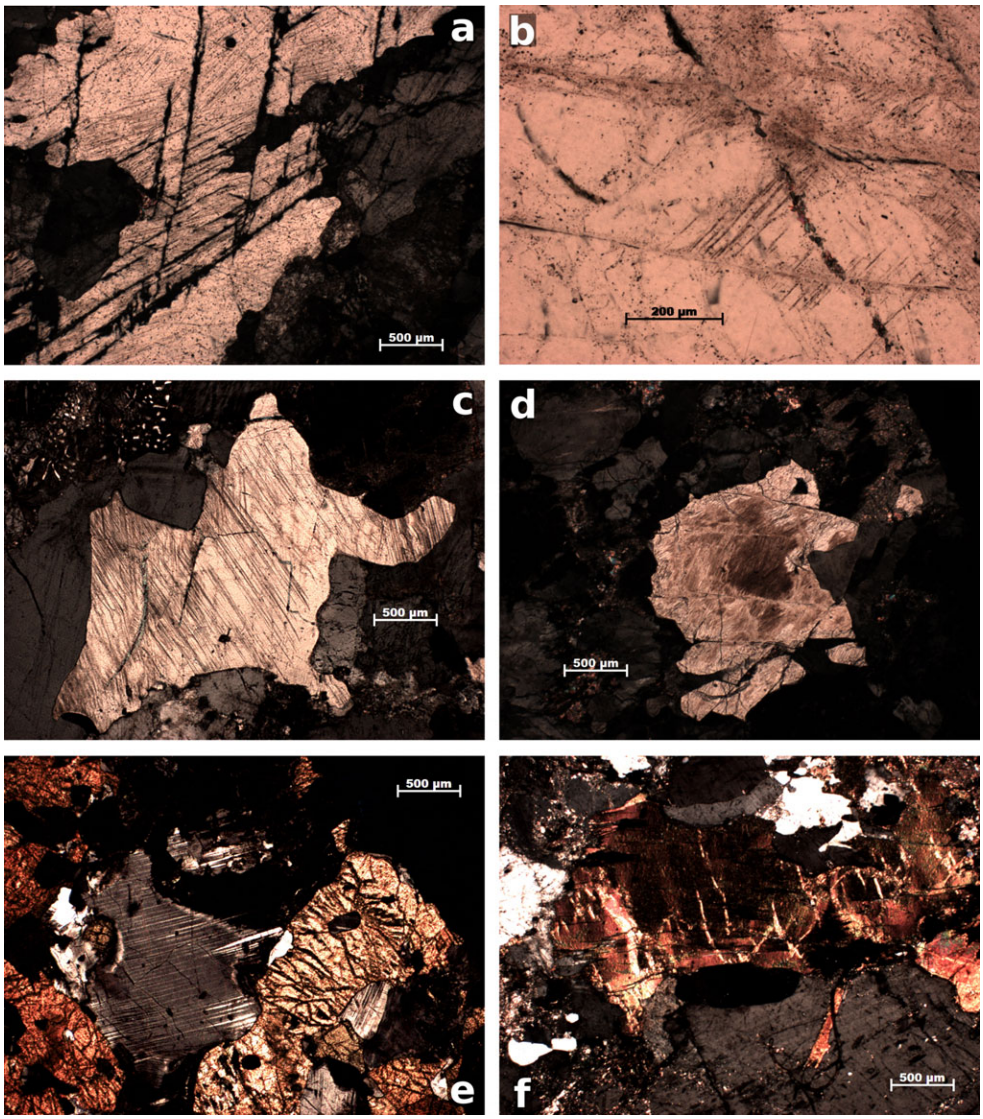

Fig. 4. Microphotograph under cross-polarized light of shock indicators from West Clearwater Lake a) Two PF sets in quartz (with three PDF sets). b) Feather Features (FFs) in quartz. c) Three sets of PDFs in quartz. d) Toasted quartz with at least two PDF sets. e) Partially diaplectic feldspar glass in mafic basement. f) Kink-banded biotite. (Color figure can be viewed at wileyonlinelibrary.com.)

Numerical Modeling

With all other parameters held constant between models, different effective viscosities, η, and decay times, T_{dec}, were used to model the West Clearwater Lake impact event. After preliminary modeling using values of η from 1×10^8 Pas to 1×10^{10} Pas, and values of T_{dec} from 7 to 600 s, it was found that the morphology of the crater could only be matched when $30 \text{ s} < T_{dec} < 120$ s. That is, when the decay time is sufficient to allow the material to be weakened long enough to facilitate collapse but is not fluidized to the extent that the structure becomes completely flat. Furthermore, effective viscosities are restricted to $6.25 \times 10^7 \text{ Pa s} < \eta < 1 \times 10^9$ Pa s.

Figure 8 shows the result of varying η between 1.25×10^8 Pa s and 1×10^9 Pa s, and T_{dec} between 30 and 90 s. Recall that, under the assumption of harmonic block oscillation with a period proportional to the block size, the characteristic block size, h, is directly proportional to η and the quality factor, Q, is proportional to η/T_{dec}.

The varying of block model parameters leads to systematic variation of crater morphology and structure. The final crater diameter varies from 34 km where $\eta = 1 \times 10^9$ Pa s and $T_{dec} = 30$ s, to 50 km, where

Table 3. Summary of PDF statistics (see Data S1).

No. of grains (n)			No. of shocked grains (n^*)			No. of measured sets (N)			No. of measured sets[a] (N^*)			Average No. of PDF sets per shocked grain (N^*/n^*)			
3405			1939			3388			3005			1.55			
Indexed PDF crystallographic orientations (absolute frequency percent[a])															
c (0001)	$\{10\bar{1}4\}$	$\{10\bar{1}3\}$[b]	$\{10\bar{1}2\}$	$\{10\bar{1}1\}$	$\{10\bar{1}0\}$	$\{11\bar{2}2\}$	$\{11\bar{2}1\}$	$\{21\bar{3}1\}$	$\{51\bar{6}1\}$	$\{11\bar{2}0\}$	$\{22\bar{4}1\}$	$\{31\bar{4}1\}$	$\{40\bar{4}1\}$	$\{51\bar{6}0\}$	Unindexed
36.5	11.5	23.1 + 4.0	4.6	1.5	0.2	1.6	0.7	1.0	1.1	0.2	0.7	0.9	0.4	0.4	11.3

[a]This is given by the total number of observed PDFs in the specific orientation divided by the total number of measured sets (N), indexed and unindexed.

[b]This orientation includes all PDFs that were indexed in the overlapping error envelopes of the $\{10\bar{1}4\}$ orientation and $\{10\bar{1}3\}$ orientation. The number of PDFs within the envelope is indicated by the additional term.

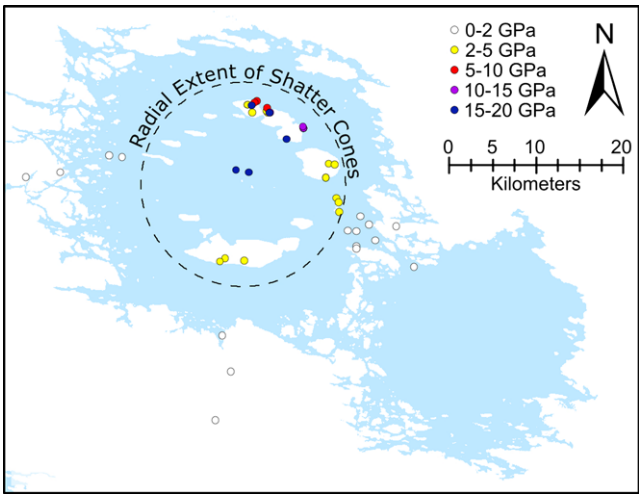

Fig. 5. Location of quartz-bearing surface samples color coded by estimated shock pressure. (Color figure can be viewed at wileyonlinelibrary.com.)

$\eta = 1.25 \times 10^8$ Pa s and $T_{dec} = 90$ s. The amount of structural uplift varies from 3 km, where $\eta = 1 \times 10^9$ Pa s and $T_{dec} = 30$ s, to 7 km, where $\eta = 1.25 \times 10^8$ Pa s and $T_{dec} = 90$ s. Structural uplift and final crater diameter increases with decreasing viscosity and increasing decay time.

Simulated drill cores and horizontal slices are constructed through the models (see Figs. 9 and 10) to allow comparison with the measured peak shock pressures. The present day level of erosion and the contact between the allochthon and para-autochthon have been selected on the basis of the topography of the crater, the position of impact-melt rocks, and the variability of shock pressure in the simulated cores. From this, the peak shock pressures in the numerical models can be directly compared to the measured peak shock data (Fig. 10).

DISCUSSION

Overall, the numerical simulations show significant variation in final crater morphology and shock distribution, when the block-model parameters, effective viscosity (η), and decay time (T_{dec}), are varied. There are several models within a tightly constrained viscosity and decay time range that share similarities with the observed shock distribution. Specifically, those models in Figs. 8–10 where $\eta = 5 \times 10^8$ Pa s and $T_{dec} = 30$ s or 60 s, or where $\eta = 2.5 \times 10^8$ Pa s and $T_{dec} = 60$ s. These models show rapid rates of shock attenuation at greater radial distances, and, in general, show the highest magnitudes of shock pressure in the center of the structure. The model that best fits the shock data (Fig. 11; Video S3 in supporting information), for

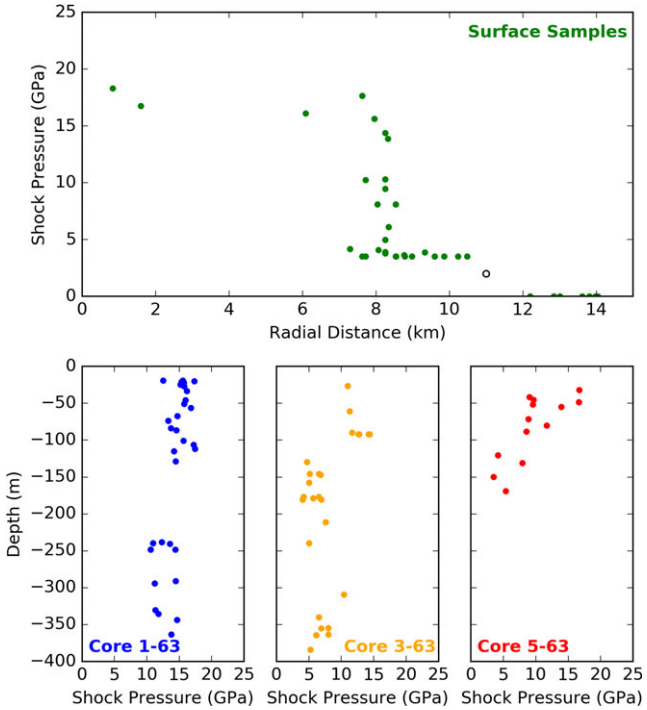

Fig. 6. Shock distribution by depth and radial distance in the three drill cores and surface samples. (Color figure can be viewed at wileyonlinelibrary.com.)

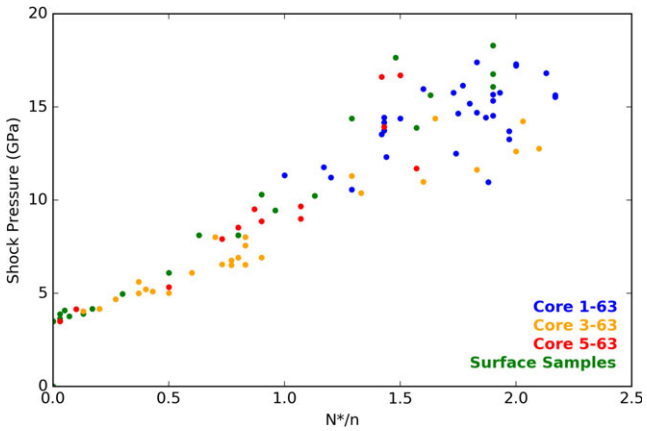

Fig. 7. Correlation between the number of PDF sets per grain (N^*/n) and the estimated peak shock pressure. (Color figure can be viewed at wileyonlinelibrary.com.)

which $\eta = 5 \times 10^8$ Pa s and $T_{dec} = 30$ s, displays a reasonable fit to the observed morphometry of the structure with a structural uplift of ~4 km. Furthermore, these values are broadly consistent with the viscosities and decay times in previous numerical modeling studies (e.g., Collins et al. 2002, 2008a; Wünnemann et al. 2005; Goldin et al. 2006).

Our best-fit viscosity and decay times are achieved using the nondimensional parameters, $\gamma_\eta = 0.025$ and

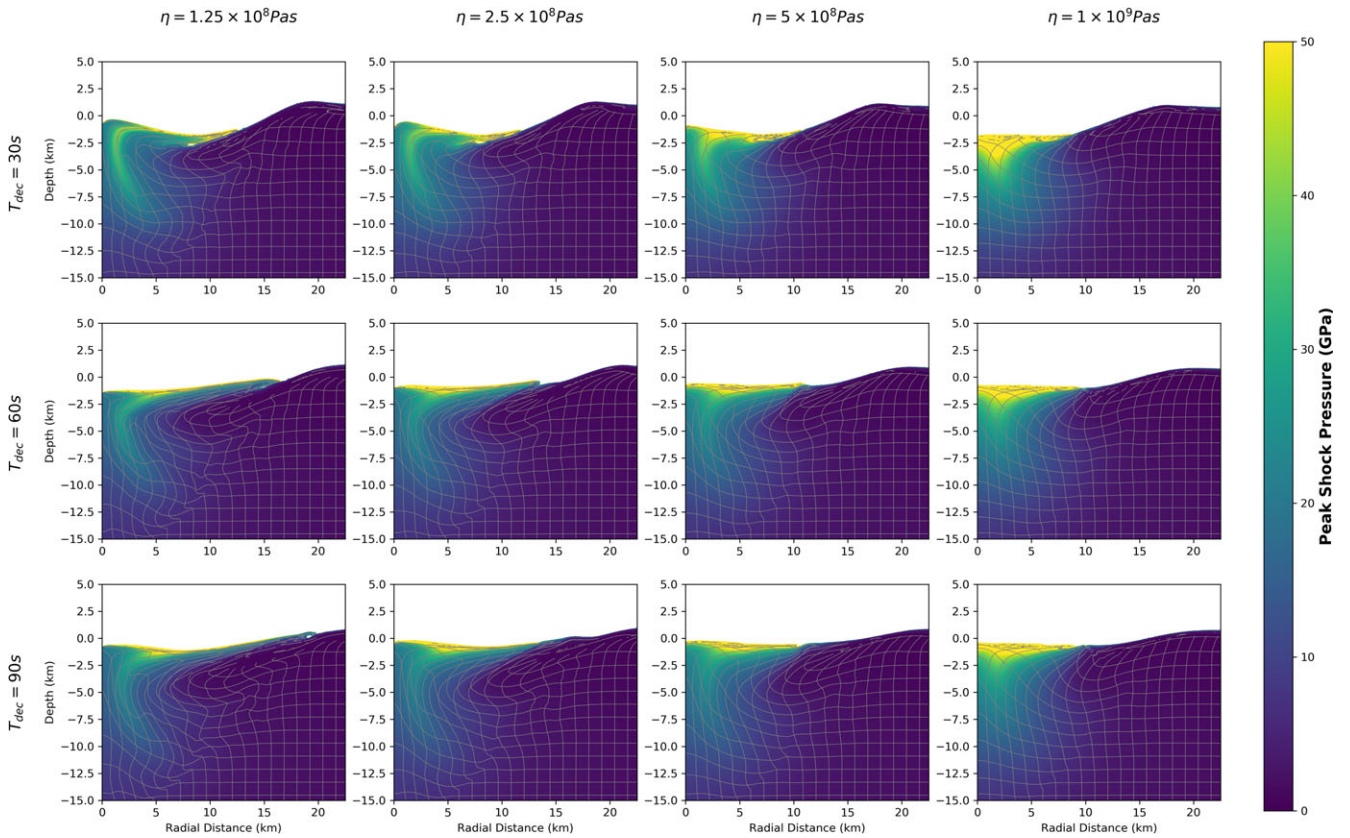

Fig. 8. The effect of varying acoustic fluidization parameters on the morphology and shock distribution of the final crater. Models are arranged with effective viscosity, η, increasing from left to right and with decay time, T_{dec}, increasing from top to bottom. Material is colored by peak shock pressure. The gray grid, with originally uniform spacing and orthogonal lines, shows the subcrater deformation. See Video S2 in supporting information. (Color figure can be viewed at wileyonlinelibrary.com.)

$\gamma_T = 100$; these values are consistent within the range of parameter values used in previous studies (Table 4). The range of γ_T values used in previous studies varies within a factor of three (115–300); our best-fit value of γ_T lies at the low-end of this range. However, while our best-fit value of γ_η is near the center of the range used in previous studies (0.008–0.2), that range encompasses two orders of magnitude. Simulations consistent with our observations would not be possible using the extreme values of γ_η in that range; that is, γ_η is restricted to $0.01 < \gamma_\eta < 0.1$, corresponding approximately to viscosities between 1×10^8 Pa s and 1×10^9 Pa s for the West Clearwater Lake structure.

Due to the trade-offs between impactor size and acoustic fluidization parameters in producing morphometrically similar craters, an absolute match between the recorded and modeled shock data is not expected in our simulations. Nonetheless, we would expect the qualitative trends in shock attenuation to be matched, a reflection of the mechanism of crater collapse. In the drill cores, our observations suggest that shock attenuates at a very low rate in the center of the structure while at 6 km radial distance, shock attenuates rapidly with depth, while shock pressures at the top of the cores and in the field samples suggest relatively high and constant shock pressures until ~8.5 km radial distance, beyond which, shock attenuates rapidly to zero (Fig. 6). The general patterns of shock attenuation in the drill cores are matched by our best-fit model, and the simulation also produces a rapid attenuation of shock pressure at radial distances beyond ~7.5 km (Fig. 11; Video S3).

We note that if, contrary to recent geochronological dating, the West Clearwater Lake structure is part of a binary doublet, that the acoustic energy from one impact may have influenced the collapse of the other crater and vice versa. The effect of interfering acoustic energy between two impacts could lead our analysis to slightly overestimate acoustic fluidization parameters, nonetheless, we would not expect that the kinematics of crater collapse to be any different. Furthermore, the shock attenuation pattern observed at West Clearwater Lake is unlikely to be affected by the East Clearwater Lake impact.

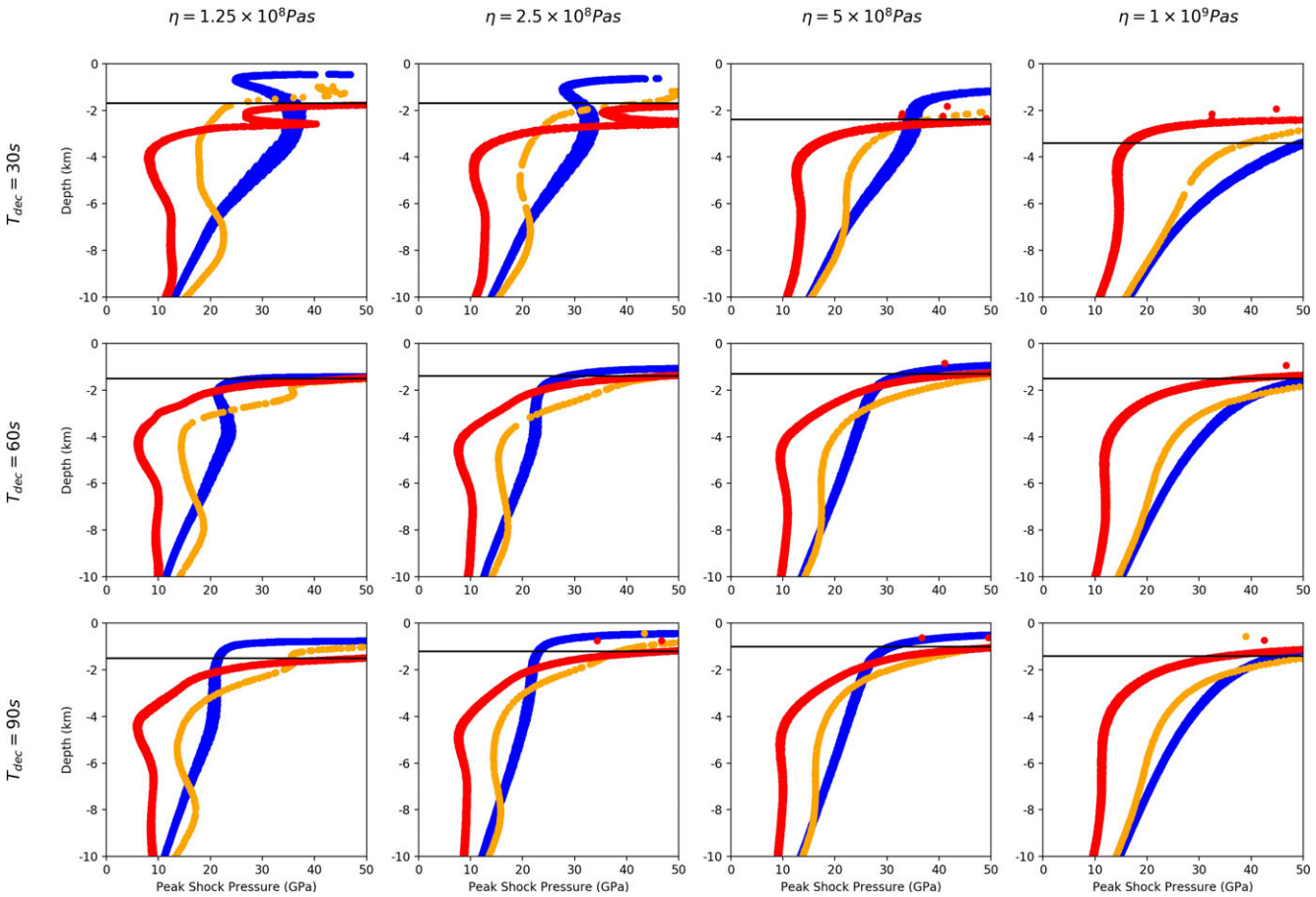

Fig. 9. Shock pressures in simulated drill cores through the numerical simulations at varying acoustic fluidization parameters. Blue, orange, and red points correspond in position to cores 1-63, 3-63, and 5-63, respectively. The interpreted position of the para-autochthonous contact in the model is indicated by the horizontal black line. (Color figure can be viewed at wileyonlinelibrary.com.)

Shock Barometry

There is an offset between the estimated and modeled peak shock pressures of ~10–20 GPa and there is considerable difference between the absolute attenuation rates in the observations compared to the numerical simulations. This can be explained in two ways (1) the numerical simulations may overestimate shock pressures and underestimate attenuation rates in natural rocks, or (2) shock pressure estimates based on PDF orientations in quartz may be inaccurate. The inaccuracy of the shock pressure estimates is likely to be due to a discrepancy between the shock pressures at which specific PDFs develop in quartz in naturally shocked rocks versus quartz in shock recovery experiments.

In this study, the estimated maximum shock pressures of ~17.5 GPa are largely due to the lack of diaplectic quartz, or devitrified diaplectic quartz glass, in any of the samples analyzed and only one occurrence of partially diaplectic feldspar glass. In the Robertson and Grieve (1977) method used here, the presence of diaplectic quartz allows for shock pressure estimates to be >27.5 GPa (Table 1). However, there is a noticeable dearth of diaplectic quartz glasses in para-autochthonous rocks across most impact structures where shock attenuation has been documented; Charlevoix (Robertson and Grieve 1977), Slate Islands (Robertson and Grieve 1977; Dressler et al. 1998), Siljan (Holm et al. 2011), and at West Clearwater Lake, while diaplectic quartz and feldspar glasses can be found at the Manicouagan (Dressler 1990) and Mistastin (Currie 1971) structures. While this pattern may be a reflection of the deeper levels of erosion at the Charlevoix, Slate Islands, and Siljan structures, West Clearwater Lake is a comparatively well preserved structure with at least half the stratigraphy of the impact-melt sheet preserved. There should be a significant volume of rock shocked between 35 GPa, commonly stated (Stöffler and Langenhorst [1994] and

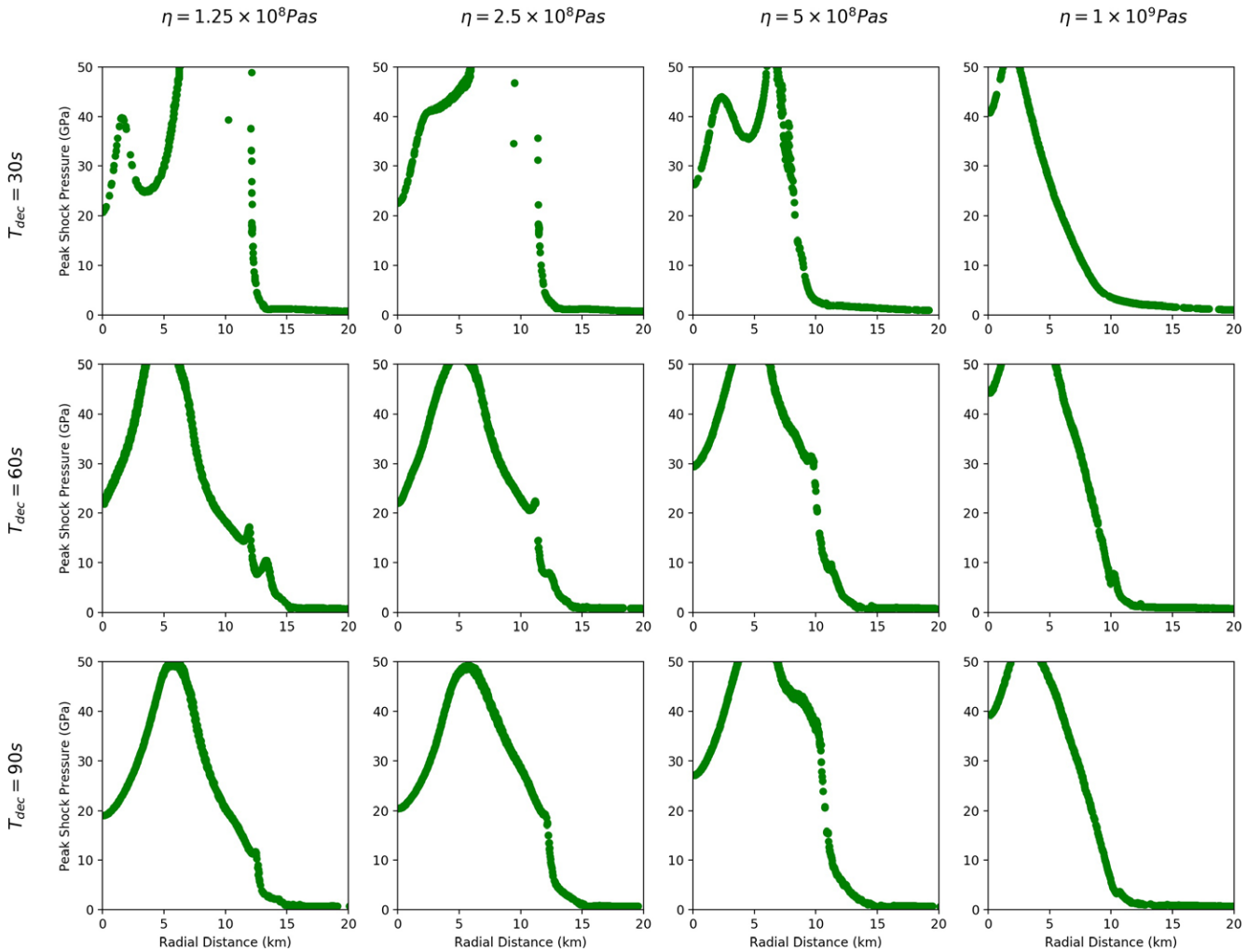

Fig. 10. Shock pressures in simulated slices through the numerical simulations corresponding to the interpreted depth at the para-autochthonous contact for each model (see Fig. 8). (Color figure can be viewed at wileyonlinelibrary.com.)

references therein) as the shock pressure for the transformation of quartz to diaplectic glass, and 50–60 GPa, where shock melting begins. Our models suggest that this volume should be ~82 km^3, which, if distributed evenly across the area up to the furthest extent of observed PDFs (~8.5 km radial distance), would be ~360 m thick. This material, which would have to be accounted for by the allochthonous breccias, only has an observed stratigraphic thickness between 0 and ~40 m (Osinski et al. 2015).

There is a significant discrepancy between the estimated and modeled peak shock pressures. However, the estimated peak shock pressures at West Clearwater Lake correlate well with the average number of PDFs per grain in each sample, considered to be a proxy of peak shock pressure (Ferrière et al. 2008). Hence, we conclude that the shock pressure estimates reliably and precisely reflect a real variation in peak shock pressure; however, the absolute value of estimated peak shock pressure may be in error.

Original Morphology

The models consistent with the shock barometry results have final crater diameters from 35–40 km where the best-fit numerical model has a final crater diameter of 35 km. Consequently, considering the uncertainties of our method, we estimate that the final crater diameter of the West Clearwater Lake impact structure was 35–40 km, which is slightly larger than the often stated 32 km apparent crater diameter based on the position of the lake shore (Dence 1964; Grieve 2006). The transient crater diameter in our simulations is ~16 km. These estimates based on the best-fit numerical model is also consistent with scaling law calculations that relate the radial extent of PDFs (8.5 km) or shatter cones

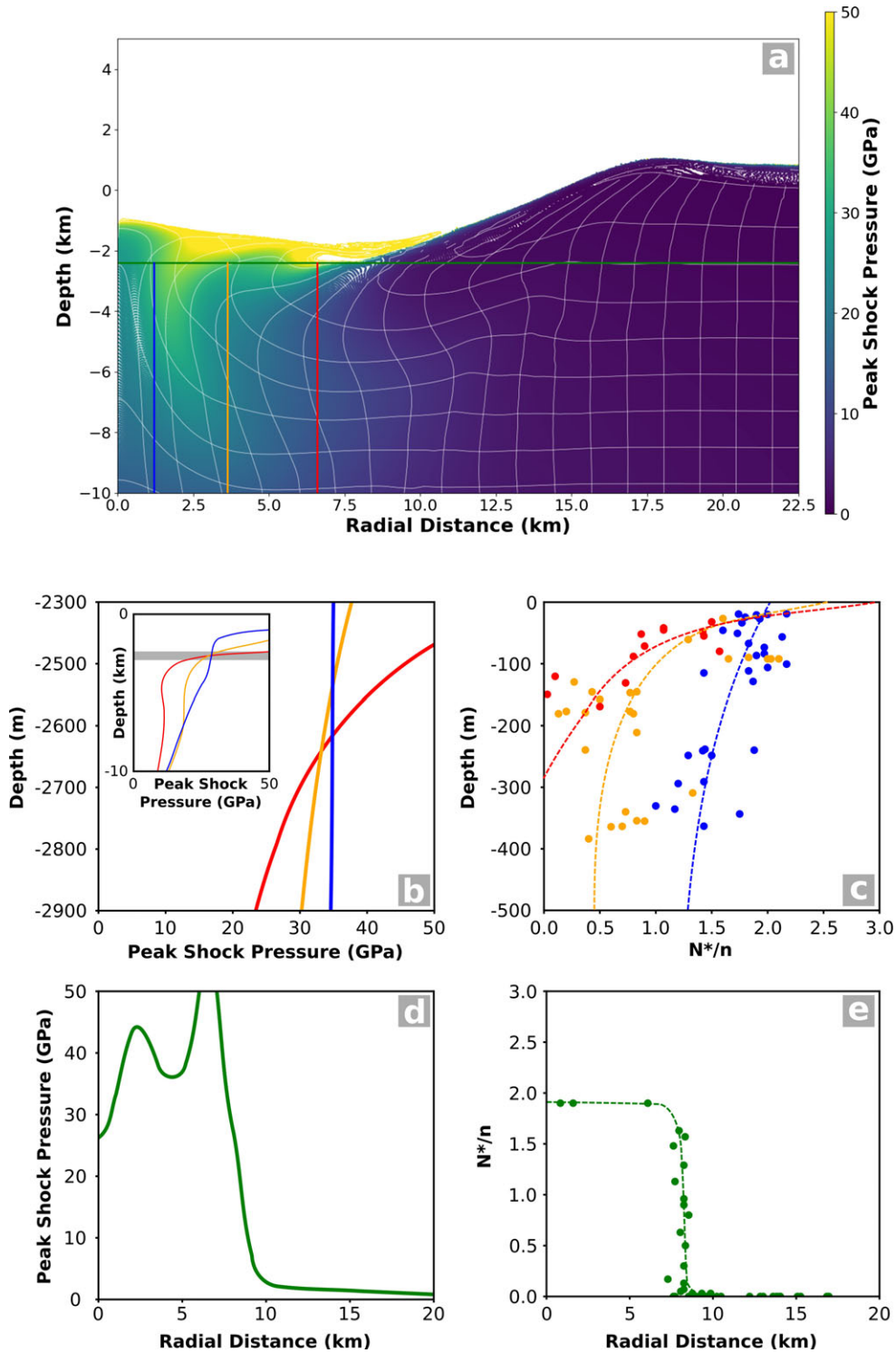

Fig. 11. a) Best fit numerical model ($\eta = 5 \times 10^8$ Pa s and $T_{dec} = 30$ s) color-shaded by peak shock pressure. Colored vertical lines at ~1 km (blue), ~4 km (orange), and ~6 km (red) radial distances correspond to simulated drill cores in (b), where peak shock pressure variation is shown with depth. This can be compared to (c), the observed shock attenuation pattern, where the average number of PDF sets per grain in a sample is shown. Dashed lines indicate the overall trends of the data. d) A simulated horizontal slice is shown, corresponding to the horizontal line (green) at ~2.4 km depth in (a). This can be compared to (e) the shock attenuation pattern in the field samples. (Color figure can be viewed at wileyonlinelibrary.com.)

Table 4. Comparison of the best-fit acoustic fluidization parameters between this and other studies.

Structure	γ_η	γ_T	Reference
West Clearwater Lake	0.025	100	This study
Lunar Peak Ring Basins	0.015	300	Baker et al. (2016)
Chesapeake Bay	0.01	120	Collins and Wünnemann (2005)
El'gygytgyn, Ries, Haughton	0.1	200	Collins et al. (2008a)
Chicxulub	0.008	115	Collins et al. (2008b)
Puchezh-Katunki	0.008	115	Collins (2014)
Sierra Madera	0.003	300	Goldin et al. (2006)
Puchezh-Katunki[a]	0.012	225	Ivanov and Artemieva (2002)
Serra da Cangalha	0.05	150	Vasconcelos et al. (2012)
Ries	0.2	300	Wünnemann et al. (2005)
Terrestrial and Lunar craters	0.1	150	Wünnemann and Ivanov (2003)

[a]Assuming an impactor diameter of 3 km (Ivanov 1994).

(11 km) to the transient cavity diameter (Dence 1972; Robertson and Grieve 1977; Stöffler et al. 1988; Osinski and Ferrière 2016), and then transient cavity diameter to final crater diameter (Grieve et al. 1981; Schenk and McKinnon 1985). Estimates based on these scaling laws produce transient crater diameters of ≥11–13 km and final crater diameters that range from 32 to 56 km.

In our best-fit numerical simulation, ~8 km radial distance marks the edge of the central uplift, beyond which, modeled shock pressure rapidly attenuates. This is a consequence of the outward movement of the central uplift over the collapsing transient cavity floor such that highly shocked material from the center of the structure slides outward over the relatively unshocked, downwardly collapsing, transient cavity floor. The observed shock attenuation pattern at West Clearwater Lake follows this pattern where shock attenuates rapidly at ~ 8.5 km radial distance.

In comparison to other impact structures, the lack of attenuation of shock pressure across the central uplift is unusual (Robertson 1975; Robertson and Grieve 1977; Dressler et al. 1998; Holm et al. 2011). This may be an effect of erosion at these other structures. In our models, deeper horizontal slices show a more gentle and continuous shock attenuation with radial distance. West Clearwater Lake is one of the least eroded structures that has been analyzed for shock attenuation; whereas, Siljan, Charlevoix, or Slate islands, with their gentler attenuation of shock pressure, are more heavily eroded structures. Erosion estimates from our three close-fit numerical models, made by comparison between estimated and predicted shock pressures, show that 1.3–2.4 km of erosion has occurred at West Clearwater Lake, relative to the preimpact topography, since the time of impact.

The shock attenuation pattern is consistent with models that show significant central-uplift collapse; however, while there is a prominent topographic peak ring at modern day exposure, the island ring seen today might not be the remnant of a topographic peak ring in the original structure. The topography of the island ring is almost entirely formed from impact-melt rock and, therefore, would have been unable, in its molten form, to support topography on the original crater. Furthermore, while some of our close-fit models do produce a subtle topographic ring or a ring shaped feature within the impact-melt sheet, the dominant topographic feature within the final crater diameter remains the central uplift, particularly so within our best-fit model. Consequently, we propose that, in its pristine condition, the West Clearwater Lake structure would have been a transitional central-peak to peak-ring crater, somewhat akin to "proto-basins" on Mercury and the Moon (Pike 1988; Baker et al. 2011a, 2011b). The erosionally resistant topographic ring structure seen today is likely to be related to concentric structure caused by the crater modification process.

Furthermore, our model provides an estimate of the impact-melt volume produced during the West Clearwater Lake impact; a total of ~90 km^3 of melt (shocked to >60 GPa) is produced of which ~62 km^3 remains within the crater to form the impact-melt sheet. This value is broadly consistent with previous impact-melt sheet volume estimates between 68–100 km^3 (Grieve et al. 1976; Phinney and Simonds 1977).

The Block Model

Our numerical models of the West Clearwater impact event are broadly consistent with morphometric observations and shock metamorphism at West Clearwater Lake. A best-fit model was achieved with parameters, $\eta = 5 \times 10^8$ Pa s and $T_{dec} = 30$ s, although an almost equivalent fit can be achieved by doubling the decay time, and halving the viscosity. These parameters can be related to observable quantities, the block size, h, and quality factor, Q (Ivanov and Artemieva 2002):

$$\eta = \frac{2\pi\rho h^2}{T} \quad \text{and} \quad T_{dec} = QT \tag{2}$$

where T is the time period of the block oscillations. Assuming the damped harmonic oscillation of blocks in compressible interblock breccia:

$$T = \frac{2\pi h}{c_s}^2 \sqrt{\frac{\rho}{\rho_b}\frac{h_b}{h}} \quad (3)$$

where ρ_b and h_b are the density and thickness of the interblock breccia, respectively. Previous studies have used the relations, $\rho_b = \rho/2$ and $h_b = 0.1 \times h$, to allow estimation of block size (Ivanov and Artemieva 2002). Fundamentally, this definition of block-oscillation period requires a significant quantity of highly compressible (i.e., low density) interblock breccia to be valid (Melosh and Ivanov 1999), which is not observed in the Clearwater Lake cores.

Using the relations $\rho_b = \rho/2$ and $h_b = 0.1 \times h$; the block size, h; and quality factor, Q; can be calculated for our models. For the best-fit model, where $\eta = 5 \times 10^8$ Pa s and $T_{dec} = 60$ s, $h = 17$ m and $Q = 3140$, although our other reasonable models (Figs. 8–10) indicates that Q could be as high as 6280. These parameters should correspond to observable characteristics in the rock record. For example, the block size (h) should correspond to the observed distance between discontinuities in the drill cores. Logging of the drill cores at West Clearwater Lake suggests that the size of individual "blocks," while variable and between <1 and ~43 m, was ~12 m on average. The drill cores only sample the upper, highly deformed portion of the para-autochthon, hence, measurements here would be expected to underestimate the "characteristic block size" parameter, h. Therefore, a value of $h = 17$ m is a reasonable value for the "characteristic block size." However, the quality factor, Q, representing the attenuation factor of acoustic energy, is considered to be somewhat analogous to the seismic quality factor of rocks (Melosh 1996); the acoustic waves of the acoustic fluidization model merely being short-wavelength seismic waves. While attenuation rates of seismic waves are frequency dependent, there is an expectation that the acoustic field should decay with a broadly similar quality factor to that of seismic waves. In crystalline rocks within a few kilometers of the surface, this value is generally between 50 and 600 (Bradley and Fort 1966; Waters 1981). The quality factor used in our best-fit simulation is an order of magnitude greater, implying that the deforming rocks during crater modification are fluidized for longer than expected. This might imply that significant regeneration of acoustic energy occurs during crater growth and collapse. Efficient regeneration of acoustic energy, which is not accounted for in the present simulations, would sustain fluidization for long enough to explain the long decay time implied by our models, while allowing small quality factors (<1000) to attenuate the acoustic field more rapidly.

On the other hand, observations from the West Clearwater Lake drill cores raise questions over the validity of the conceptual model of a stiff block oscillating in compressible breccia and, hence, the simple scaling between T_{dec}, η, h, T, and Q. Our drill core logging suggests that $\frac{\rho}{\rho_b} = 2$ and $\frac{h_b}{h} = 0.1$ are not reasonable assumptions at West Clearwater Lake. Instead, we find that $\frac{h_b}{h} \leq 0.01$, and while direct measurements of the densities of discontinuities and rock blocks were not made, a more realistic constraint is $\frac{\rho}{\rho_b} \leq 1.1$. Using these more realistic values together with our best-fit model parameters only increases Q to a value to ~30,000, while reducing the block size, h, to 4 m. Similar issues with the block model have been raised at other impact structures, for example, Haughton (Osinski et al. 2005). Importantly, the observation of interblock breccia thicknesses less than 1% of the block size brings into question the applicability a model based on damped harmonic oscillation of independently oscillating blocks in breccia.

The combination of the unrealistic value of the quality factor parameter and the inconsistencies between observations and the justification of the block model leads us to the conclusion that the block model, while capable of producing a rheology of deforming material to explain the morphology of complex craters, cannot be used to directly constrain physical parameters, such as block size. Despite some uncertainty in the absolute values of the acoustic fluidization parameters, largely due to trade-offs with impactor parameters, it is clear that the assumption of a uniform block size with distance from the crater center in the current block model implementation is an oversimplification (e.g., Kenkmann et al. 2006). A treatment of the full acoustic fluidization model, as described by (Melosh 1979), which makes no assumption about the presence of significant interblock breccias and which prolongs weakening in strongly deforming regions may provide better justification for the collapse of large impact structures. These factors may qualitatively change the kinematics of crater collapse in numerical simulations to better reflect the process of central uplift formation.

CONCLUSIONS

Shock pressure estimates from observations of PDFs in quartz-bearing lithologies at West Clearwater Lake show that peak shock pressures are fairly constant across the central uplift, with a maximum value in the center of the structure of at least 17.5 GPa. Shock pressure attenuates more rapidly with depth at greater radial distances.

This shock distribution pattern can be explained by the outward collapse of a highly shocked central-uplift over downwardly and inwardly collapsing, weakly shocked crater rim. The kinematics of numerical impact

simulations using the block model of acoustic fluidization are capable of qualitatively matching this shock distribution, while remaining consistent with the geologically observable morphology of the crater.

The conceptual idea behind the justification of the block model of acoustic fluidization lacks observational support at West Clearwater Lake. The assumption that the deforming "interblock breccia" is significantly compressible and present in "large" volumes is not supported by observations of deformation zones in the drill cores. In addition, while the block model succeeds in reproducing the kinematics of complex crater collapse, it does not appear to be possible to relate the parameters to observable quantities. One possible explanation for this disconnect is that regeneration of acoustic vibrations during the cratering process, which is not accounted for in the present implementation of the block model, is important in prolonging acoustic fluidization, allowing complete crater collapse.

The original final crater (rim) diameter of the West Clearwater Lake impact structure is estimated to be 35–40 km. Subsequent differential erosion of the structure has led to up to ~2 km of denudation (relative to the preimpact topography), removing all impact ejecta and at least half the thickness of the impact-melt sheet. The impact-melt volume estimated by our numerical simulations is ~90 km^3, of this, ~62 km^3 remains within the crater cavity to form an impact-melt sheet. These estimates are consistent with previous estimates of the original impact-melt volume at West Clearwater Lake. We suggest that the original morphology of the structure was a transitional central-peak–peak-ring crater.

Acknowledgments—ASPR gratefully acknowledges the assistance in the field from the University of Western Ontario team; R. Wilks, M. Kerrigan, R. Misener, A. Coulter, and D. Saint-Jacques along with the NASA FINESSE project. The contributions of R. Wilks and M. Kerrigan were greatly appreciated while logging the drill cores. We are grateful for the constructive reviews of S. Holm-Alwmark and K. Wünnemann that helped to improve the manuscript. We gratefully acknowledge the developers of iSALE (www.isale-code.de). This work was funded by STFC (ST/J001260/1).

Editorial Handling—Michael Poelchau

REFERENCES

Amsden A. A., Ruppel H. M., and Hirt C. W. 1980. SALE: A simplified ALE computer program for fluid flow at all speeds. (No. LA-8095). New Mexico: Los Alamos National Laboratories.

Baker D. M. H., Head J. W., Fassett C. I., Kadish S. J., Smith D. E., Zuber M. T., and Neumann G. A. 2011a. The transition from complex crater to peak-ring basin on the Moon: New observations from the Lunar Orbiter Laser Altimeter (LOLA) instrument. *Icarus* 214:377–393. doi:10.1016/j.icarus.2011.05.030.

Baker D. M. H., Head J. W., Schon S. C., Ernst C. M., Prockter L. M., Murchie S. L., Denevi B. W., Solomon S. C., and Strom R. G. 2011b. The transition from complex crater to peak-ring basin on Mercury: New observations from MESSENGER flyby data and constraints on basin formation models. *Planetary and Space Science* 59:1932–1948. doi:10.1016/j.pss.2011.05.010.

Baker D. M. H., Head J. W., Collins G. S., and Potter R. W. K. 2016. The formation of peak-ring basins: Working hypotheses and path forward in using observations to constrain models of impact-basin formation. *Icarus* 273:146–163. doi:10.1016/j.icarus.2015.11.033.

Beals C. S., Ferguson G. M., and Landau A. 1956. A Search for analogies between lunar and terrestrial topography on photographs of the Canadian Shield. *Journal of the Royal Astronomical Society of Canada* 50:203–250.

Biren M. B., van Soest M. C., Wartho J.-A., Hodges K. V., and Spray J. G. 2016. Diachroneity of the Clearwater West and Clearwater East impact structures indicated by the (U–Th)/He dating method. *Earth and Planetary Science Letters* 453:56–66. doi:10.1016/j.epsl.2016.07.053.

Bostock H. H. 1969. The Clearwater Complex, New Quebec. *Geological Survey of Canada, Bulletin* 178:63.

Bradley J. J. and Fort A. N. 1966. Internal friction in rocks. In *Handbook of physical constants*, edited by Clark S. P. *Geological Society of America Memoir* 97:173–193.

Carter N. L. 1965. Basal quartz deformation lamellae; a criterion for recognition of impactites. *American Journal of Science* 263:786–806. doi:10.2475/ajs.263.9.786.

Chapman C. R. and McKinnon W. B. 1986. Cratering of planetary satellites. In *Satellites*, edited by Burns J. A. and Matthews M. S. Tucson, Arizona: The University of Arizona Press. pp. 492–580.

Collins G. S. 2014. Numerical simulations of impact crater formation with dilatancy. *Journal of Geophysical Research Planets* 119:2600–2619. doi:10.1002/2014JE004708.

Collins G. S. and Wünnemann K. 2005. How big was the Chesapeake Bay impact? Insight from numerical modeling. *Geology* 33:925–928. doi:10.1130/G21854.1.

Collins G. S., Melosh H. J., Morgan J. V., and Warner M. R. 2002. Hydrocode simulations of Chicxulub Crater collapse and peak-ring formation. *Icarus* 157:24–33. doi:10.1006/icar.2002.6822.

Collins G. S., Kenkmann T., Osinski G. R., and Wünnemann K. 2008a. Mid-sized complex crater formation in mixed crystalline-sedimentary targets: Insight from modeling and observation. *Meteoritics & Planetary Science* 43:1955–1977. doi:10.1111/j.1945-5100.2008.tb00655.x.

Collins G. S., Morgan J., Barton P., Christeson G. L., Gulick S., Urrutia J., Warner M., and Wünnemann K. 2008b. Dynamic modeling suggests terrace zone asymmetry in the Chicxulub crater is caused by target heterogeneity. *Earth and Planetary Science Letters* 270:221–230. doi:10.1016/j.epsl.2008.03.032.

Currie K. L. 1971. Geology of the resurgent cryptoexplosion crater at Mistastin Lake, Labrador. *Geological Survey of Canada, Bulletin* 207:62.

Dence M. R. 1964. A comparative structural and petrographic study of probable Canadian meteorite craters. *Meteoritics* 2:249–270. doi:10.1111/j.1945-5100.1964.tb01432.x.

Dence M. R. 1972. Meteorite impact craters and the structure of the Sudbury Basin. New Dev. Sudbury Geol. *Geological Association of Canada Special Paper* 10:117–124.

Dence M. R. 2004. Structural evidence from shock metamorphism in simple and complex impact craters: Linking observations to theory. *Meteoritics & Planetary Science* 39:267–286. doi:10.1111/j.1945-5100.2004.tb00340.x.

Dence M. R., Innes M. J. S., and Beals C. S. 1965. On the probable meteorite origin of the Clearwater Lakes, Quebec. *Journal of the Royal Astronomical Society of Canada* 59:13–22.

Dressler B. 1990. Shock metamorphic features and their zoning and orientation in the Precambrian rocks of the Manicouagan Structure, Quebec, Canada. *Tectonophysics* 171:229–245. doi:10.1016/0040-1951(90)90101-D.

Dressler B. O., Sharpton V. L., and Schuraytz B. C. 1998. Shock metamorphism and shock barometry at a complex impact structure: Slate Islands, Canada. *Contributions to Mineralogy and Petrology* 130:275–287. doi:10.1007/s004100050365.

Elbeshausen D., Wünnemann K., and Collins G. S. 2009. Scaling of oblique impacts in frictional targets: Implications for crater size and formation mechanisms. *Icarus* 204:716–731. doi:10.1016/j.icarus.2009.07.018.

Engelhardt W. von and Bertsch W. 1969. Shock induced planar deformation structures in quartz from the Ries crater, Germany. *Contributions to Mineralogy and Petrology* 20:203–234. doi:10.1007/BF00377477.

Engelhardt W. von, Hörz F., Stöffler D., and Bertsch W. 1968. Observations on quartz deformation in the breccias of West Clearwater Lake, Canada and the Ries Basin, Germany. In *Shock metamorphism of natural materials*, edited by French B. M. and Short N. M. Baltimore, Maryland: Mono Book Corporation. pp. 475–482.

Ferrière L., Koeberl C., Ivanov B. A., and Reimold W. U. 2008. Shock metamorphism of Bosumtwi impact crater rocks, shock attenuation, and uplift formation. *Science* 322:1678–1681. doi:10.1126/science.1166283.

Ferrière L., Morrow J. R., Amgaa T., and Koeberl C. 2009. Systematic study of universal-stage measurements of planar deformation features in shocked quartz: Implications for statistical significance and representation of results. *Meteoritics & Planetary Science* 44:925–940. doi:10.1111/j.1945-5100.2009.tb00778.x.

French B. M. and Koeberl C. 2010. The convincing identification of terrestrial meteorite impact structures: What works, what doesn't, and why. *Earth Science Reviews* 98:123–170. doi:10.1016/j.earscirev.2009.10.009.

Goldin T. J., Wünnemann K., Melosh H. J., and Collins G. S. 2006. Hydrocode modeling of the Sierra Madera impact structure. *Meteoritics & Planetary Science* 41:1947–1958. doi:10.1111/j.1945-5100.2006.tb00462.x.

Grieve R. A. F. 1978. Meteoritic component and impact melt composition at the lac à l'Eau Claire (Clearwater) impact structures, Quebec. *Geochimica et Cosmochimica Acta* 42:429–431. doi:10.1016/0016-7037(78)90275-2.

Grieve R. A. F. 2006. *Impact Structures in Canada, GEOtext 5*. St. John's, Newfoundland: Geological Association of Canada. 210 p.

Grieve R. A. F. and Robertson P. B. 1976. Variations in shock deformation at the Slate Islands impact structure, Lake Superior, Canada. *Contributions to Mineralogy and Petrology* 58:37–49. doi:10.1007/BF00384743.

Grieve R. A. F., Dence M. R., and Robertson P. B. 1976. The generation and distribution of impact melts: Implications for cratering processes. LPI Contribution 259. Houston, Texas: Lunar and Planetary Institute. 40 p.

Grieve R. A. F., Robertson P. B., and Dence M. R. 1981. Constraints on the formation of ring impact structures, based on terrestrial data. In *Proceedings of the conference on multi-ring basins: Formation and evolution*, edited by Merrill R. B. and Schultz P. H. New York: Pergamon Press. pp. 37–57.

Grieve R. A. F., Langenhorst F., and Stöffler D. 1996. Shock metamorphism of quartz in nature and experiment: II. Significance in geoscience. *Meteoritics & Planetary Science* 31:6–35. doi:10.1111/j.1945-5100.1996.tb02049.x.

Hische R. 1994. *Geology of the Clearwater impact structure (English translation)*. Münster: Westphalian Wilhelm University. 200 p.

Holm S., Alwmark C., Alvarez W., and Schmitz B. 2011. Shock barometry of the Siljan impact structure, Sweden. *Meteoritics & Planetary Science* 46:1888–1909. doi:10.1111/j.1945-5100.2011.01303.x.

Hörz F. 1968. Statistical measurements of deformation structures and refractive indices in experimentally shock loaded quartz. In *Shock metamorphism of natural materials*, edited by French B. M. and Short N. M. Baltimore, Maryland: Mono Book Corporation. pp. 243–253.

Huber M. S., Ferrière L., Losiak A., and Koeberl C. 2011. ANIE: A mathematical algorithm for automated indexing of planar deformation features in quartz grains. *Meteoritics & Planetary Science* 46:1418–1424. doi:10.1111/j.1945-5100.2011.01234.x.

Huffman A. R. and Reimold W. U. 1996. Experimental constraints on shock-induced microstructures in naturally deformed silicates. *Tectonophysics* 256:165–217. doi:10.1016/0040-1951(95)00162-X.

Ivanov B. A. 1994. Geomechanical models of impact cratering Puchezh-Katunki structure. In *Large meteorite impacts and planetary evolution*, edited by Dressler B. O., Grieve R. A. F., and Sharpton V. L. GSA Special Paper 293. Boulder, Colorado: Geological Society of America. pp. 81–91.

Ivanov B. A. 2005. Numerical modeling of the largest terrestrial meteorite craters. *Solar System Research* 39:381–409. doi:10.1007/s11208-005-0051-0.

Ivanov B. A. and Artemieva N. A. 2002. Numerical modeling of the formation of large impact craters. *Geological Society of America Special Paper* 356:619–630. doi:10.1130/0-8137-2356-6.619.

Ivanov B. A. and Kostuchenko V. N. 1997. Block oscillation model for impact crater collapse (abstract #631). 28th Lunar and Planetary Science Conference. CD-ROM.

Ivanov B. A., Kocharyan G. G., Kostuchenko V. N., Kirjakov A. F., and Pevzner L. A. 1996. Puchezh-Katunki Impact Crater: Preliminary data on recovered core block structure (abstract #589). 27th Lunar and Planetary Science Conference. CD-ROM.

Ivanov B. A., Deniem D., and Neukum G. 1997. Implementation of dynamic strength models into 2D hydrocodes: Applications for atmospheric breakup and impact cratering. *International Journal of Impact Engineering* 17:375–386. doi:10.1016/S0734-743X(97)87511-2.

Kenkmann T., Jahn A., and Wünnemann K. 2006. "Block size" in a complex impact crater inferred from the Upheaval Dome Structure, Utah (abstract #1540). 37th Lunar and Planetary Science Conference. CD-ROM.

Kenkmann T., Collins G. S., Wittmann A., Wünnemann K., Reimold W. U., and Melosh H. J. 2009. A model for the formation of the Chesapeake Bay impact crater as revealed by drilling and numerical simulation. *Geological Society of America Special Paper* 458:571–585. doi:10.1130/2009.2458(25).

Kenkmann T., Collins G. S., and Wünnemann K. 2012. The modification stage of crater formation. In *Impact cratering*, edited by Osinski G. R. and Pierazzo E. Chichester, UK: John Wiley & Sons, Ltd. pp. 60–75.

Kranck S. H. and Sinclair G. W. 1963. Clearwater Lake, New Quebec. Geological Survey of Canada Bulletin 100. 25 p.

Le Feuvre M. and Wieczorek M. A. 2011. Nonuniform cratering of the Moon and a revised crater chronology of the inner solar system. *Icarus* 214:1–20. doi:10.1016/j.icarus.2011.03.010.

McKinnon W. B. 1978. An investigation into the role of plastic failure in crater modification. Proceedings, 9th Lunar and Planetary Science Conference. pp. 3965–3973.

Melosh H. J. 1977. Crater modification by gravity—A mechanical analysis of slumping. In *Impact and explosion cratering*, edited by Roddy D. J., Pepin R. O., and Merrill R. B. New York: Pergamon Press. pp. 1245–1260.

Melosh H. J. 1979. Acoustic fluidization: A new geologic process? *Journal of Geophysical Research Solid Earth* 84:7513–7520. doi:10.1029/JB084iB13p07513.

Melosh H. J. 1989. *Impact cratering: A geologic process, Oxford monographs on geology and geophysics*. New York: Oxford University Press.

Melosh H. J. 1996. Dynamical weakening of faults by acoustic fluidization. *Nature* 379:601–606. doi:10.1038/379601a0.

Melosh H. J. and Ivanov B. A. 1999. Impact crater collapse. *Annual Review of Earth and Planetary Sciences* 27:385–415. doi:10.1146/annurev.earth.27.1.385.

Melosh H. J., Ryan E. V., and Asphaug E. 1992. Dynamic fragmentation in impacts: Hydrocode simulation of laboratory impacts. *Journal of Geophysical Research Planets* 97:14,735–14,759. doi:10.1029/92JE01632.

Müller W. F. and Défourneaux M. 1968. Deformationsstrukturen im Quartz als Indikator für Stosswellen: Eine experimentelle Untersuchung an Quartz-Einkristallen. *Zeitschrift fur Geophysik* 34:483–504.

O'Keefe J. D. and Ahrens T. J. 1999. Complex craters: Relationship of stratigraphy and rings to impact conditions. *Journal of Geophysical Research Planets* 104:27,091–27,104. doi:10.1029/1998JE000596.

Osinski G. R. and Ferrière L. 2016. Shatter cones: (Mis) understood? *Science Advances* 2:e1600616. doi:10.1126/sciadv.1600616.

Osinski G. R., Lee P., Spray J. G., Parnell J., Lim D. S. S., Bunch T. E., Cockell C. S., and Glass B. 2005. Geological overview and cratering model for the Haughton impact structure, Devon Island, Canadian High Arctic. *Meteoritics & Planetary Science* 40:1759–1776. doi:10.1111/j.1945-5100.2005.tb00145.x.

Osinski G. R., Brunner A., Cohen B. A., Coulter A., Elphic R., Grieve R. A. F., Heldmann J. L., Hodges K., Horne A., Kerrigan M., Lim D. S. S., Misener R., Morgan J. V., Rae A. S. P., Saint-Jacques D., Skok J. R., Squyres S., Tornabene L. L., Wilks R., and Young K. 2015. Revisiting the West Clearwater Lake Impact Structure, Canada (abstract #1621). 46th Lunar and Planetary Science Conference. CD-ROM.

Palme H., Janssens M.-J., Takahashi H., Anders E., and Hertogen J. 1978. Meteoritic material at five large impact craters. *Geochimica et Cosmochimica Acta* 42:313–323. doi:10.1016/0016-7037(78)90184-9.

Phinney W. C. and Simonds C. H. 1977. Dynamical implications of the petrology and distribution of impact melt rocks. In *Impact and explosion cratering*, edited by Roddy D. J., Pepin R. O., and Merrill R. B. New York: Pergamon Press. pp. 771–790.

Phinney W. C., Simonds C. H., Cochran A., and McGee P. E. 1978. West Clearwater, Quebec Impact Structure, Part II: Petrology. Proceedings, 9th Lunar and Planetary Science Conference. pp. 2659–2694.

Pierazzo E., Vickery A. M., and Melosh H. J. 1997. A Reevaluation of impact melt production. *Icarus* 127:408–423. doi:10.1006/icar.1997.5713.

Pike R. J. 1988. Geomorphology of impact craters on Mercury. In *Mercury*, edited by Vilas F., Chapman C. R., and Shapley-Matthews M. Tucson, Arizona: The University of Arizona Press. pp. 165–273.

Reimold W. U., Grieve R. A. F., and Palme H. 1981. Rb-Sr dating of the impact melt from East Clearwater, Quebec. *Contributions to Mineralogy and Petrology* 76:73–76. doi:10.1007/BF00373685.

Robertson P. B. 1975. Zones of shock metamorphism at the Charlevoix impact structure, Quebec. *Geological Society of America Bulletin* 86:1630–1638. doi:10.1130/0016-7606(1975)86<1630:ZOSMAT>2.0.CO;2.

Robertson P. B. and Grieve R. A. F. 1977. Shock attenuation at terrestrial impact structures. In *Impact and explosion cratering*, edited by Roddy D. J., Pepin R. O., and Merrill R. B. New York: Pergamon Press. pp. 687–702.

Rosa D. F. 2004. *Marble enclaves in the melt sheet at the West Clearwater Lake Impact Crater, Northern Quebec*. Montreal: McGill University. 147 p.

Rosa D. F. 2011. *The sheet of impact melt at West Clearwater Lake, Northern Quebec*. Montreal: McGill University. 392 p.

Schenk P. M. and McKinnon W. B. 1985. Dark halo craters and the thickness of grooved terrain on Ganymede. *Journal of Geophysical Research Solid Earth* 90:C775–C783. doi:10.1029/JB090iS02p0C775.

Schmieder M., Schwarz W. H., Trieloff M., Tohver E., Buchner E., Hopp J., and Osinski G. R. 2015. New 40Ar/39Ar dating of the Clearwater Lake impact structures (Québec, Canada) – Not the binary asteroid impact it seems? *Geochimica et Cosmochimica Acta* 148:304–324. doi:10.1016/j.gca.2014.09.037.

Simonds C. H., Phinney W. C., McGee P. E., and Cochran A. 1978. West Clearwater, Quebec impact structure, Part I: Field geology, structure and bulk chemistry. Proceedings, 9th Lunar and Planetary Science Conference. pp. 2633–2693.

Stöffler D. and Langenhorst F. 1994. Shock metamorphism of quartz in nature and experiment: I. Basic observation and theory. *Meteoritics* 29:155–181. doi:10.1111/j.1945-5100.1994.tb00670.x.

Stöffler D., Bischoff L., Osierski W., and Wiest B. 1988. Structural deformation, breccia formation, and shock metamorphism in the basement of complex terrestrial impact craters: Implications for the cratering process. *Deep Drilling in Crystalline Bedrock* 1:277–297.

Thompson S. L. and Lauson H. S. 1974. Improvements in the CHART D radiation-hydrodynamic code III: Revised analytic equations of state (No. SC-RR-710714). Alberquerque, New Mexico: Sandia National Laboratory.

Vasconcelos M. A. R., Wünnemann K., Crósta A. P., Molina E. C., Reimold W. U., and Yokoyama E. 2012. Insights into the morphology of the Serra da Cangalha impact structure from geophysical modeling. *Meteoritics & Planetary Science* 47:1659–1670. doi:10.1111/maps.12001.

Waters K. H. 1981. *Reflection seismology: A tool for energy resource exploration*, 2nd ed. New York: John Wiley & Sons, Ltd.

Wilks R. P. A. and Osinski G. R. 2015. Impact melt veins in the Central Uplift of the West Clearwater Lake Impact Structure, Northern Quebec, Canada (abstract #1397). 46th Lunar and Planetary Science Conference. CD-ROM.

Wünnemann K. and Ivanov B. A. 2003. Numerical modelling of the impact crater depth–diameter dependence in an acoustically fluidized target. *Planetary and Space Science* 51:831–845. doi:10.1016/j.pss.2003.08.001.

Wünnemann K., Morgan J. V., and Jödicke H. 2005. Is Ries crater typical for its size? An analysis based upon old and new geophysical data and numerical modeling. *Geological Society of America Special Paper* 384:67–83. doi:10.1130/0-8137-2384-1.67.

Wünnemann K., Collins G. S., and Melosh H. J. 2006. A strain-based porosity model for use in hydrocode simulations of impacts and implications for transient crater growth in porous targets. *Icarus* 180:514–527. doi:10.1016/j.icarus.2005.10.013.

SUPPORTING INFORMATION

Additional supporting information may be found in the online version of this article:

Data S1. Full PDF statistics.

Video S1. Animation, Variation of crater process by varying impactor diameter, and maintaining constant acoustic fluidisation parameters.

Video S2. Animation of Figure 8, The effect of varying acoustic fluidization parameters on the morphology and shock distribution of the final crater.

Video S3. The Animation of Figure 11a. Best fit numerical model, color-shaded by peak shock pressure.